The correct analysis of shocks in a cellular material

J.J. Harrigan, S.R. Reid, A. Seyed Yaghoubi

▶ **To cite this version:**

J.J. Harrigan, S.R. Reid, A. Seyed Yaghoubi. The correct analysis of shocks in a cellular material. International Journal of Impact Engineering, 2010, 37 (8), pp.918. 10.1016/j.ijimpeng.2009.03.011 . hal-00699209

HAL Id: hal-00699209
https://hal.science/hal-00699209

Submitted on 20 May 2012

HAL is a multi-disciplinary open access archive for the deposit and dissemination of scientific research documents, whether they are published or not. The documents may come from teaching and research institutions in France or abroad, or from public or private research centers.

L'archive ouverte pluridisciplinaire **HAL**, est destinée au dépôt et à la diffusion de documents scientifiques de niveau recherche, publiés ou non, émanant des établissements d'enseignement et de recherche français ou étrangers, des laboratoires publics ou privés.

Accepted Manuscript

Title: The correct analysis of shocks in a cellular material

Authors: J.J. Harrigan, S.R. Reid, A. Seyed Yaghoubi

PII: S0734-743X(09)00061-X

DOI: 10.1016/j.ijimpeng.2009.03.011

Reference: IE 1766

To appear in: *International Journal of Impact Engineering*

Received Date: 16 September 2008

Revised Date: 19 March 2009

Accepted Date: 23 March 2009

Please cite this article as: Harrigan JJ, Reid SR, Seyed Yaghoubi A. The correct analysis of shocks in a cellular material, International Journal of Impact Engineering (2009), doi: 10.1016/j.ijimpeng.2009.03.011

This is a PDF file of an unedited manuscript that has been accepted for publication. As a service to our customers we are providing this early version of the manuscript. The manuscript will undergo copyediting, typesetting, and review of the resulting proof before it is published in its final form. Please note that during the production process errors may be discovered which could affect the content, and all legal disclaimers that apply to the journal pertain.

ARTICLE IN PRESS

The correct analysis of shocks in a cellular material

J. J. Harrigan[1*], S. R. Reid[1], A. Seyed Yaghoubi[2]

[1] School of Engineering, Fraser Noble Building,
King's College, University of Aberdeen, Aberdeen AB24 3UE, U.K.
[2] School of Mechanical, Aerospace & Civil Engineering,
Pariser Building, University of Manchester, PO Box 88, Manchester M60 1QD, U.K.

Abstract

Cellular materials have applications for impact and blast protection. Under impact/impulsive loading the response of the cellular solid can be controlled by compaction (or shock, see [3, 4]) waves. Different analytical and computational solutions have been produced to model this behaviour but these solutions provide conflicting predictions for the response of the material in certain loading scenarios. The different analytical approaches are discussed using two simple examples for clarity. The differences between apparently similar "models" are clarified. In particular, it is argued that mass-spring models are not capable of modelling the discontinuities that exist in a compaction wave in a cellular material.

Keywords: *Cellular material; Compaction wave; Shock wave.*

ACCEPTED MANUSCRIPT

[*] Corresponding author. Tel :+44(0)1224 272512; fax : +44(0)1224 272497;
e-mail : j.harrigan@abdn.ac.uk

1. Introduction

Cellular materials (e.g. foams, honeycombs *etc*.) are employed in many applications due to their multi-functional properties, including insulation and low weight, especially for packaging and in light-weight sandwich panels. One of their applications is as an energy absorbing layer for impact and blast protection. The cellular materials considered here are those that are characterised by a relatively flat plateau stress until densification. As such, they are often considered to be ideal energy absorbers because of their low weight and their ability to deform over a long stroke at an almost constant load (see Fig. 1). During quasi-static compression the energy absorbed per unit volume is equal to the area under the nominal stress-strain curve, i.e. the cellular material is considered as a continuum, not a material comprising the edges and faces of the actual cell structure. However, under intense dynamic loads the cellular structure plays a key role and compaction waves propagating through the cellular array play an important role in the response of cellular solids. The compression is localized at discontinuity (shock) fronts and deformations propagate through the cells in a progressive manner. Various methods have been proposed to model "shock wave" (more precisely "compaction front") propagation in cellular solids, e.g. one-dimensional shock wave models (e.g. [1-9]), spring–mass models [10, 11] and FE modelling (e.g. [7-9]). In addition one-dimensional 'shock wave' models have been applied to certain loading scenarios but with different formulations [12-14] of the "shock theory". The different analytical approaches have led to some debate, e.g. [15-17].

The aim of this article is not to present a new method. Rather it is to provide clarity in a very confused area by comparing three existing methods for the analysis of dynamic

ACCEPTED MANUSCRIPT

compaction of cellular materials. These methods are: (i) “shock theory”; (ii) “energy conservation”; (iii) mass-spring models. The comparison is carried out by considering the solutions to two idealised loading scenarios (Examples 1 and 2 defined later). The different assumptions inherent to each method are shown to lead to large differences between the predictions.

Reid and Peng [1] provided the first “shock wave” predictions for cellular solids to explain certain experimental results, focusing on the enhancement of the crushing strength of wood specimens. For simplicity, the cellular solid was idealized as a rigid, perfectly-plastic, locking (*R-P-P-L*) material. Developments of the same simple shock theory have been applied with more accurate material models in order to predict better the stresses during direct impact testing of cellular solids. For example, an elastic, plastic, hardening material model was used in [5, 6]. Lopatnikov et al. [8, 9] used an ‘‘elastic–perfectly–plastic–rigid’’ model and shock-wave analysis to predict the deformation of aluminium foam in both foam projectile [8] and target [9] tests. For the simple “shock” wave analysis used in [1-4] the strain is equal to one of two possible values, *viz.* zero or a value associated with the fully locked material. In [8, 9] the effect of elasticity is incorporated but the strain within the compacted material is again given a value associated with the fully locked material, although the locking strain is defined in a different way. However the basic assumptions in the analysis remain and provide good agreement with FE predictions [8, 9]. The predictions in [1-9] differ only in detail (see [17]) and will be grouped together as “shock wave” models.

ACCEPTED MANUSCRIPT

FE modelling of the dynamic compaction of cellular solids has been carried out in two ways. In certain investigations the material has been treated as a continuum [7-9]. In other simulations approximations to the actual structure of either two-dimensional [4, 20-21] or three-dimensional [22] cellular solids are modelled. As continuum-based FE predictions have been shown to agree with "shock wave" theory, they are discussed only briefly here.

An alternative solution to dynamic loading of foams wherein the deformation is governed by a compaction wave was reported in [12] giving the equation of motion and energy absorption for the case of a rigid mass striking a foam column. This formulation has since been repeated or used in [13, 14, 18], and discussed in [15, 16]. In [12, 13] the case of a rigid mass striking a foam layer with the distal face fixed rigidly was considered. In [14] the analysis was extended to that of a sandwich panel by considering the overall motion of both face-sheets and the compression of the internal foam layer when the panel is subjected to blast. The procedure used in [14] was then applied to a clamped, circular sandwich plate in [18] to predict the energy absorbed and timescales associated with the core compression stage.

Tan *et al* [4] argued that the equations of motion derived in [12] are incorrect. The "steady-state shock" equations in [4] were derived from a thermo-mechanical approach. Whilst providing useful insights, this approach clouds the simplicity of a derivation based on a purely mechanical approach using conservation of mass and momentum only. In this paper, this simpler approach is used in order to illustrate the essence of the 'shock' model for impact/blast loading and to clarify certain features of the solution of such problems that have appeared in the recent literature, two examples are presented. In Example 1, conservation of momentum is applied to

ACCEPTED MANUSCRIPT

predict the compaction of an energy absorbing foam column which is struck by a rigid mass as shown in Fig. 2, i.e. the same example as in [12]. In doing so, it will be made clear that the solutions based on "shock wave" models [1-9] are fundamentally different to those based on the formulations in [12-14, 18]. The *R-P-P-L* idealisation is used for Example 1. The aim is to derive the governing equations in a simpler way than in [4] as well as to illustrate the differences between the "shock wave" theory and the predictions in either [10, 11] or [12], rather than to predict more accurately experimental data, which will be the subject of a future paper. In the *R-P-P-L* model quasi-static material behaviour is characterised by two parameters, i.e. the plateau stress σ_P and the locking (densification) strain ε_D.

Example 2 builds on the theory developed in Example 1 to explain the large differences between the predictions of mass-spring models described in [10, 11] and "shock theory". In Example 2, the boundary condition corresponding to the impact of a rigid mass on the foam column (example 1) is replaced by a constant pressure applied over a short duration. The intensive pressure pulse load from a blast is another possible source for shock propagation in a cellular material. Li and Meng [10] studied the "compressive shock wave propagation in the solid phase of a cellular material" using a one-dimensional mass-spring model. A foam column was subjected to a rectangular pressure pulse at one end (simplified 'blast' loading) while the other end was fixed to a rigid support. Stress enhancement (i.e. stresses greater than the applied pressure [10]) within the foam was predicted during the propagation of the compaction wave through the cellular material. Further, a series of pressure pulses were considered in order to predict the critical pulses delivered to the foam core, beyond which the maximum pressure pulse applied to the rigid support was greater

ACCEPTED MANUSCRIPT

than the original, applied pressure. An *R-P-P-L* idealisation is again used to obtain closed-form solutions. A more realistic elastic, perfectly plastic, hardening (*E-P-P-H*) material description is used later for one loading scenario for comparison with the *R-P-P-L* model and the results in [10].

Gao and Yu [11] used a one-dimensional mass-spring system to model the response of a cellular material to a short duration pressure pulse in order to investigate the effect of material properties on the response. The speed of the compaction wave predicted by the mass-spring model is shown to agree well with that predicted by "shock theory" [11]. However, typical pressures considered in [10] were 2 to 5 times the plateau stress in the material whereas in [11] the maximum pressure considered is only 2.5 times the "collapse stress" of the material. Additionally, Li and Meng provide an attenuation/enhancement boundary in [10] (discussed in Example 2) that is not provided in [11]. For these reasons, the predictions in [10] are used for comparison in Example 2.

2. Example 1: Compaction wave in cellular solid subject to impact by a rigid mass

Under a high speed impact or high magnitude impulsive load, a cellular material deforms in a progressive manner with the cells adjacent to the loaded surface compacting first and the deformation then passing through the material in a wave-like manner. Whilst this problem has been treated previously (e.g. [6, 7], for clarity, the steps in developing the basic theory are repeated below.

The dynamic crushing model for a rigid projectile of mass G striking a *R-P-P-L* target of mass M_{Core}, initial length l_0, cross-sectional area A_0 and density ρ_0 is illustrated in

ACCEPTED MANUSCRIPT

Fig. 2. The mass G has an initial velocity v_0 and strikes the cellular column at time t = 0. Fig. 2 (a) shows the situation just before impact while Figs. 2 (b) and (c) illustrate the compression at times t and $t + \delta t$. As cellular solids can undergo large plastic compression in one direction without lateral expansion, the target is assumed to deform under uniaxial compressive strain conditions. As the compaction wave travels through the material a strong discontinuity is assumed to exist between the deformed and undeformed regions. In the undeformed region ahead of the wave, the stress is equal to the plateau stress σ_P (essentially assuming an infinite elastic wave speed) while the strain and particle velocity there are zero. After compression the stress can take any value. The compacted region travels with the same (reducing) velocity as the mass and has been compressed to the densification strain, ε_D . The stress in this region is now considered.

From kinematic considerations it can be shown [1] that the speed of the compaction front relative to the projectile (see Fig. 2) is

$$\frac{dx}{dt} = \frac{1-\varepsilon_D}{\varepsilon_D} v, \tag{1}$$

where v is the instantaneous velocity of the rigid mass with respect to a stationary frame. Conservation of mass [1] gives

$$\frac{\rho_0}{\rho_D} = 1-\varepsilon_D = \frac{x}{x+u}, \tag{2}$$

where ρ_0 is the initial density, ρ_D is the density when fully crushed, u is the displacement of the rigid mass at time t, and x is the deformed length of the crushed cellular material. Over a small time interval δt (see Fig. 2) the compaction wave travels along the column so that a small element of material of mass δm is added to

ACCEPTED MANUSCRIPT

the front of the compacted portion which increases in length by a small amount δx. The mass of this element is

$$\delta m = \frac{\rho_0 A_0 \delta x}{1-\varepsilon_D}. \tag{3}$$

Over the time interval δt this element has stresses σ_D and σ_P on its left and right faces respectively, where σ_D is the stress just inside the compacted region. The element has zero velocity at time t and a velocity v at time $t + \delta t$. Conservation of momentum for the element of mass δm over the time increment δt during which it undergoes compaction gives

$$(\sigma_D - \sigma_P) A_0 \delta t = v \delta m. \tag{4}$$

Substituting Eqns. (1) and (2) into (4) leads to

$$\sigma_D = \sigma_P + \frac{\rho_0}{\varepsilon_D} v^2. \tag{5}$$

This is the original, simple, stress enhancement formula (c.f. [1]) for the stress just inside the discontinuity and can also be derived by applying the classical Rankine-Hugoniot relationships (e.g. [4]). All the referenced works use this equation in one form or another. However, after this point different models diverge. In Section 3.1, conservation of momentum is applied to the whole system to derive an equation of motion. In Section 3.2, the alternative "energy balance" approach is employed to derive a different equation of motion.

3. Two different solution schemes in the literature

ACCEPTED MANUSCRIPT

3.1 Scheme 1: "Conservation of momentum" approach

Conservation of momentum for the whole system shown in Fig. 2 over the period from t to $t + \delta t$ gives

$$\left[G + \rho_D (x + \delta x) A_0\right]\left[v + \delta v\right] - \left[G + \rho_D x A_0\right] v = -\sigma_P A_0 \delta t \,. \tag{6}$$

Thus, substituting Eqns. (1) and (2) into Eqn. (5), the governing equation of motion is

$$\frac{dv}{dt} = \frac{d^2 u}{dt^2} = v\frac{dv}{du} = -\left(\sigma_P + \frac{\rho_0}{\varepsilon_D} v^2\right) \Bigg/ \left[\frac{G}{A_0} + \frac{\rho_0}{\varepsilon_D} u\right]. \tag{7}$$

Integrating Eqn. (7) with the initial condition $v = v_0$ at $u = 0$ gives

$$v = \sqrt{\frac{\varepsilon_D}{\rho_0}\left[\left(\left(\frac{\rho_0}{\varepsilon_D} v_0^2 + \sigma_P\right)\left(\frac{G}{A_0}\right)^2 \Bigg/ \left(\frac{G}{A_0} + \frac{\rho_0}{\varepsilon_D} u\right)^2\right) - \sigma_P\right]}. \tag{8}$$

Thus for $\sigma_D > \sigma_P$, from Eqns. (5) and (8) the stress just behind the compaction front can be found as a function of the displacement of the rigid mass, i.e.

$$\sigma_D = \left(\frac{\rho_0}{\varepsilon_D} v_0^2 + \sigma_P\right)\left(\frac{G}{A_0}\right)^2 \Bigg/ \left(\frac{G}{A_0} + \frac{\rho_0}{\varepsilon_D} u\right)^2 . \tag{9}$$

The compaction front will continue to propagate through the foam until either the mass is brought to rest or the compaction front reaches the distal end, which results in rigid impact with the support for the *R-P-P-L* shock model. The impact velocity, v_D, for which the cellular specimen is just fully crushed before the end mass is brought to rest, can be found by setting the initial velocity as $v_0 = v_D$ and the final velocity as $v = 0$ when $u = u_{\max}$ in Eqn. (8), i.e.

ACCEPTED MANUSCRIPT

$$v_D = \sqrt{\frac{\sigma_P \varepsilon_D}{\rho_0}\left[\left(1+\frac{A_0\rho_0 u_{\max}}{G\varepsilon_D}\right)^2 - 1\right]}. \tag{10}$$

The maximum displacement of the proximal end is $u_{\max} = l_0\varepsilon_D$, where l_0 is the original length of the column. Therefore, equation (10) can be written in terms of the mass ratio for full specimen locking as

$$v_D = \sqrt{\frac{\sigma_p \varepsilon_D}{\rho_0}\left[\left(1+\frac{M_{core}}{G}\right)^2 - 1\right]}, \tag{11}$$

where M_{core} is the mass of the cellular material cylinder. It follows that for full locking of the specimen, the ratio of the specific energy absorbed under conditions where the response is governed by the propagation of a compaction (structural shock) wave to that under quasi-static compression is given by

$$\psi = \frac{M_{core}}{2G} + 1. \tag{12}$$

Equation (12) shows that for impacting masses with equal kinetic energy but different masses (and impact velocities), the ratio of the specific energy absorption can be defined in terms of the mass ratio only. This clearly demonstrates the shock enhancement in the dynamic energy absorbing mechanism. Additionally, from equation (11) we can find the critical length of the foam column required to just bring a mass G with an impact velocity v_0 to rest as

$$l_{CR1} = \frac{G}{\rho_0 A_0}\left(\sqrt{1+\frac{\rho_0 v_0^{\,2}}{\sigma_P \varepsilon_D}} - 1\right). \tag{13}$$

3.2 Scheme 2: "Energy balance" approach

ACCEPTED MANUSCRIPT

However a different development of the equations is found in [12-14]. Assuming that the energy absorbed during the dynamic compression is equal to that for quasi-static compression as in [12-14], "*conservation of energy"* for the element of mass δm over the time increment δt during which it undergoes compaction (Fig. 2) gives

$$\sigma_D = \sigma_P + \frac{\rho_0}{2\varepsilon_D} v^2 . \tag{14}$$

A similar "energy conservation" approach for the whole system between times *t* and *t* + δt (Fig. 2) gives,

$$\left[G + \rho_D A_0 x\right] v \delta v + \frac{1}{2} \rho_D A_0 v^2 \delta x = \sigma_P \varepsilon_D A_0 \delta l . \tag{15}$$

Substituting Eqns. (1) and (2) into Eqn. (15), the governing equation of motion is

$$\frac{dv}{dt} = v\frac{dv}{du} = -\left(\sigma_P + \frac{\rho_0}{2\varepsilon_D} v^2\right) \Big/ \left[\frac{G}{A_0} + \frac{\rho_0}{\varepsilon_D} u\right]. \tag{16}$$

Integrating Eqn. (16) with the initial conditions $v = v_0$ at $u = 0$ gives,

$$v = \sqrt{\frac{2\varepsilon_D}{\rho_0}\left[\left(\frac{\sigma_P + \frac{\rho_0 v_0^2}{2\varepsilon_D}}{1 + \frac{\rho_0 A_0 u}{G\varepsilon_D}}\right) - \sigma_P\right]} . \tag{17}$$

From this "energy balance" approach the impact velocity that just causes full crushing of the core by the end mass can be found either by setting $v_0 = v_D$ and $v = 0$ when $u = u_{\max}$ in Eqn. (17), or more simply by equating the initial kinetic energy of the mass with the maximum energy absorbed by the cellular column, giving

$$v_D = \sqrt{\frac{2A_0 u_{\max} \sigma_P}{G}} . \tag{18}$$

ACCEPTED MANUSCRIPT

It follows that the critical thickness of cellular solid required to just bring a mass G with an impact velocity v_0 to rest is

$$l_{CR} = \frac{G{v_0}^2}{2A_0\sigma_P\varepsilon_D}. \tag{19}$$

That is, $\psi = 1$ and, as expected, there is no velocity effect on energy absorption.

3.3 Comparison of the solution schemes 1 and 2

It should be noted that Eqn. (5) and Eqn. (7) are consistent and that Eqn. (7) can be derived from Eqn. (5) by considering the motion of the end mass and compressed material to the left of the shock front. In the same way Eqns. (14) and (16) form a consistent pair in that Eqn. (16) can be derived from Eqn. (14). However, solution Scheme 2 violates momentum conservation for both the prediction of the stress just inside the compaction front (*c.f.* Eqns. (14) and (5)) and the governing equation of motion (*c.f.* Eqns. (16) and (7)); therefore Scheme 2 is incorrect. In Scheme 1 no assumptions are made regarding the energy absorption capacity of the column of cellular material whereas this was done in Scheme 2. Energy *is* conserved in Scheme 1 and not in scheme 2 despite the "energy balance" approach used, as can be illustrated by considering the hatched element in Fig. 2. Over the time increment δt, the work done on this element by external forces is

$$W_E = \sigma_D A_0 \delta u, \tag{20}$$

and the gain in kinetic energy of the element is

$$T_E = \frac{1}{2}\frac{A_0\rho_0 v^2\delta x}{\left(1-\varepsilon_D\right)}. \tag{21}$$

By conservation of energy, the energy absorbed by plastic deformation per unit volume of the element is therefore

ACCEPTED MANUSCRIPT

$$E_V = \frac{1}{2}(\sigma_D + \sigma_P)\varepsilon_D . \quad (22)$$

Eqn. (22) is consistent with the Scheme 1 solution and can be derived from the Rankine-Hugoniot jump conditions, as has been done elsewhere [4]. *The key point is that the conservation equations that should be applied when dealing with wave motion that involves discontinuities in density, particle velocity and stress, refer to initial and final values across the shock and are not a function of the path between the initial and final values.* This creates no problem for equations involving mass and momentum conservation. The assumption in Scheme 2 that the energy absorbed per unit volume is equal to the area under the stress-strain curve (i.e. $E_V = \sigma_P \varepsilon_D$) is erroneous as this clearly implies that the material follows a certain path during the compression. The correct "energy balance" approach would be to use the Rankine-Hugoniot equation that ensures energy conservation across a discontinuity. Scheme 1 makes no assumptions regarding path-dependency and agrees with the "shock theory" in [1-9]. However, the differences between solutions available in the literature are not so apparent as the differences between Schemes 1 and 2 above. That is because in [12-14, 18] Eqn (5) is used to describe the stress jump across the shock. However, the equation of motion used in [12-14, 18] corresponds to the Scheme 2 approach, i.e. Eqn. (16).

The differences between the two solutions is illustrated in Fig. 3, which shows the critical length of a foam column struck by a 40 kg.m^{-2} mass over a range of velocities according to Eqns. (13) and (19). The *R-P-P-L* foam properties used in the analysis are given in the figure title. Clearly the differences between solution Schemes 1 and 2 become large with increasing impact velocity. Note that no energy absorbing mechanism has been defined that is a function of strain-rate or velocity, yet Scheme 1

ACCEPTED MANUSCRIPT

analysis predicts that the energy absorbed increases with increasing impact velocity (substitute for σ_D from Eqn. (5) in Eqn. (22)).

4. Example 2: Comparison between mass-spring models and "shock wave" predictions for a foam column subjected to high pressure over a short duration

The use of foam has been suggested as a possible way of mitigating blast loads. This important application has been modelled using mass-spring idealisation in recent work [10]. There are several interesting features in this application of cellular materials for blast protection including a possible shock *enhancement* resulting from the use of a "protective" foam layer. Such an event is problematic and counterintuitive, considering the use of such a foam as a protective measure.

The experimental evidence for this enhancement was discussed in [10], and in that paper, the characteristics of compressive shock wave propagation in a cellular material were treated using a one-dimensional mass-spring model. For illustrative purposes, the foam core was considered to be subjected to a rectangular pressure pulse at one end with magnitude P and duration T (see Fig. 4), while the other end of the foam core was fixed and this simplification is followed herein for comparison purposes.

Typical pressures considered were 2 to 5 times the plateau stress in the material and it was argued in [10] that, although a one-dimensional mass-spring model is more suitable for a system consisting of periodic structures, such as a ring or tube system, it is still capable of representing a macroscopically continuous cellular material. The three stage stress-strain curve used in [10] is shown in Fig. 1. The material response is first linear elastic, then perfectly-plastic before hardening begins at a "lock-up" strain.

ACCEPTED MANUSCRIPT

The findings were that stress enhancement may occur during the propagation of a compaction wave through a cellular material [10], where stress enhancement was defined as stresses anywhere along the foam column that are greater than the applied pressure. Additionally it was shown that the conditions for full densification of the mass-spring system (i.e. compression of every spring beyond the "lock-up" strain) and conditions for blast enhancement at the rigid support (i.e. loads greater than the applied load) are almost the same. A series of pressure pulses were considered in order to predict the pulse conditions for full densification and therefore stress enhancement at the rigid support. This is shown in Fig. 5 in non-dimensional form where

$$p = \frac{P}{\sigma_P}\ , \tag{23}$$

$$\tau_d = \frac{T}{L}\sqrt{\frac{E}{\rho_0}}, \tag{24}$$

and E is the elastic modulus of the foam core.

For the same loading condition, it is straighforward to use "shock theory" with an *R-P-P-L* material model (see [7] for similar example). The pressure pulse is applied at $t = 0$ and there are two distinct stages to the solution.

Stage 1: $t < T$. The boundary condition during this stage is that there is a high pressure P at the left end of the column. This is essentially the same loading condition as considered by Tan et al [4] to derive the "steady state shock model". In this stage there is a steady-shock with the two states on either side of the shock remaining constant with time. The compaction wave starts from the loaded end and the stress

ACCEPTED MANUSCRIPT

within this compacted region is raised to *P*. From Eqn. (5), the particle velocity behind the shock during stage 1 is

$$v_I = \sqrt{\frac{\varepsilon_D}{\rho_0}\left(P - \sigma_P\right)}. \tag{25}$$

At time $t = T$, there is a compacted portion at the left end of the column with an undeformed length given by

$$l_I = T\frac{v_I}{\varepsilon_D}. \tag{26}$$

From Eqns. (25) and (26),

$$l_I = \frac{T}{\varepsilon_D}\sqrt{\frac{\varepsilon_D}{\rho_0}\left(P - \sigma_P\right)} \tag{27}$$

Stage 2: This is equivalent to Example 1, with a mass *G* impacting the foam column of length l_{II}, where $G = \rho_0 A_0 l_I$, and $l_{II} = l - l_I$ is the undeformed length of the foam at time $t = T$. The mass ratio of the foam core to the rigid mass is equal to the ratio of l_{II} to l_I. So, considering only the critical case where the length l_{II} is fully compacted at the end of stage 2, Eqn (11) gives

$$\frac{l_{II}}{l_I} = \sqrt{1 + \frac{\rho_0 v_I^2}{\sigma_P \varepsilon_D}} - 1. \tag{28}$$

Since the total critical length of the column in this scenario is $l_{CR2} = l_I + l_{II}$ and substituting for the velocity from Eqn. (25) and for l_I from Eqn. (27), the critical initial length of the foam column can be defined in terms of the loading parameters and material properties as

$$l_{CR2} = T\sqrt{P\frac{\left(P - \sigma_P\right)}{\sigma_P \rho_0 \varepsilon_D}}. \tag{29}$$

ACCEPTED MANUSCRIPT

Because Eqn. (29) is defined for an *R-P-P-L* material, it is not possible to non-dimensionalise the solution as has been done in [10]. However, the two predictions can be compared by approximating the properties used in [10] for Rohacell 51 WF foam reported in [19]. For this material, the properties are summarised in Table 1, the only difference between the properties in Table 1 and those tabulated in [19] is that, following [10], the material is assumed to be linear-elastic up to the plateau stress so that the yield strain ε_Y is equal to 3.64%. Therefore, taking a column length of 1 m for simplicity, a dimensionless loading period $\tau_d = 1$ corresponds to a loading time of 1.53 ms.

For the "shock theory" model the material is assumed to be *R-P-P-L* with a plateau stress of 0.8 MPa and a locking strain of 68.9%. Eqn. (29) can be rearranged so that for an initial length of 1 m, the critical period of loading for a given pressure can be calculated from,

$$T_{CR} = \sqrt{\frac{\sigma_P \rho_0 \varepsilon_D}{P(P-\sigma_P)}}\,. \tag{30}$$

Eqn. (30) has been used to plot the enhancement/attenuation boundary for a 1 m long column of Rohacell 51 WF in Fig. 6. Both of the curves in Fig. 6 separate the pressure pulses that lead to shock enhancement at the distal boundary due to full compaction of the foam core from those pulses that are attenuated by the foam. The regions above and to the right of the lines experience enhancement. The differences between the two predictions are extremely large. The material model used in [10] incorporates both elasticity and a hardening régime beyond the densification strain (defined as "lock-up" strain in [10]). This more accurate material description requires an extended shock model which is dealt with in the next sub-section.

ACCEPTED MANUSCRIPT

4.1 Shock-wave models based on *R-P-P-L* and *E-P-P-H* material descriptions

The generation of attenuation/enhancement boundaries from shock theory is more difficult when using an *E-P-P-H* material model than is the case for the *R-P-P-L* idealisation. A single case is used to illustrate the effect of the inclusion of elasticity and hardening beyond the onset of densification. The *R-P-P-L* idealisation used here employs a locking strain definition that is consistent with that in [2, 3]. However, this definition is unrealistic for large velocity changes wherein the stress jump is large and strain jumps can be significantly greater than the locking strain defined in Fig. 1. The locking strain used in the previous section and in [2, 3] is essentially the strain at the onset of densification (see [23]) and its use for more intense shocks will in general lead to an over-prediction of stresses due to compaction waves (see [4, 24]).

In order to consider a shock wave model based on a fuller *E-P-P-H* material description, it is necessary to generalise the basic equations for the theory given above, following [6]. Consider a one-dimensional, compressive shock wave propagating through a cellular material as illustrated in Fig. 7. At the shock front there is a discontinuous change in properties. The material state ahead of the shock is denoted by subscript *A* and the compacted material behind the shock has the subscript *B*. Conservation of mass and momentum across the shock gives:

$$v_B - v_A = c_S\left(1 - \frac{\rho_A}{\rho_B}\right), \tag{31}$$

$$\sigma_B - \sigma_A = c_S \rho_A \left(v_B - v_A\right), \tag{32}$$

where v is absolute particle velocity and c_S is the shock speed relative to the material just ahead of the shock, so that the absolute shock speed is

ACCEPTED MANUSCRIPT

$$V_S = v_A + c_S \,. \tag{33}$$

Using the more general form of Eqn. (2) to define the density ρ in terms of strain ε,

$$\rho(\varepsilon) = \frac{\rho_0}{1-\varepsilon}, \tag{34}$$

from Eqn. (31) the shock speed is given by (see [6, 17])

$$c_S = \frac{[v]}{[\varepsilon]}(1-\varepsilon_A) = \frac{\delta Z}{\delta t} \ , \tag{35}$$

where [] denotes the change in quantity across the shock front and Z is the displacement of the shock front (used later) relative to the particle displacement just ahead of the shock and is defined according to Eqn. (35) such that a steady shock with a speed c_S would traverse a length δZ of material ahead of the shock over a time increment δt. The mass of material δm that is compacted by the shock over this time increment can therefore be calculated using

$$\frac{\delta m}{\delta t} = A_0 \rho_A c_S = A_0 \rho_0 \frac{[v]}{[\varepsilon]} = A_0 \rho_A \frac{\delta Z}{\delta t} \,. \tag{36}$$

Combining Eqns. (31) and (32) gives

$$[\sigma] = \frac{\rho_0 [v]^2}{[\varepsilon]} \,. \tag{37}$$

The *E-P-P-H* material model used here is based on that used in [10]. The elastic and perfectly-plastic parts of the stress-strain response are the same (see Fig. 1) as those in [10]. However, for compression beyond the densification strain, a slightly different and more convenient stress-strain relationship than that in [10] is used. This is because the densification behaviour defined in [10] according to Eqn. (38) below is difficult to incorporate in the set of differential equations that must be solved for the extended shock-wave solution:

ACCEPTED MANUSCRIPT

$$\sigma(\varepsilon) = 1 + \beta\left[\tan\left(\frac{\pi}{2}\left((1-\gamma)+\gamma\frac{\varepsilon-\varepsilon_D}{1-\varepsilon_D}\right)\right) - \tan\left(\frac{\pi}{2}(1-\gamma)\right)\right] \quad (38)$$

To incorporate an approximate hardening behaviour for the *E-P-P-H* model, consider a compaction wave travelling through the foam, with the material ahead of the foam already loaded to the elastic limit by an elastic wave. Eqns. (37) and (38) have been combined to plot the relationship between the particle velocity jump across the compaction front and the strain just inside the compaction front in Fig. 8. Note that Eqn. (38) is in terms of strain whereas Eqn. (37) is in terms of strain jump. However, converting from absolute strain to strain jump is simple as the strain ahead of the compaction wave is ε_Y. In Fig. 8, the *E-P-P-H* behaviour is a straight line approximation of the curve derived from Eqn. (38) and is given by

$$\varepsilon = \varepsilon_D + 0.00105[v]. \quad (39)$$

Note that equation (39) relates the change in particle velocity to the change in strain (from ε_D to ε) through the gradient of the straight line in Fig. 8. The constant in equation (39) therefore has units of $m^{-1}.s$. Based on the two curves plotted in Fig. 8 and Eqn. (35), it is possible to plot a relationship between the shock speed and the change in particle velocity. This is plotted for both the material defined by Eqn (38) and the *E-P-P-H* models in Fig. 9. Clearly there is little difference between the shock properties of the two material models. Eqn. (37) was used to plot a stress-strain curve for the *E-P-P-H* material model. From Fig. 1 it can be seen that this *E-P-P-H* model is a reasonable approximation to the material model used in [10] and defined in Eqn. (38).

4.1.1 Stage 1 for *E-P-P-H* shock wave model

ACCEPTED MANUSCRIPT

As with the *R-P-P-L* solution, the *E-P-P-H* analysis is carried out in two stages. Unfortunately, it is not possible to obtain closed-form solutions for the *E-P-P-H* material model. For illustration, a single case is considered for comparison with the predictions in [10]. The case considered is for an applied pressure P of 3.6 MPa (non-dimensional pressure $p = 4.5$). A foam column of 1 m in length is assumed so that the non-dimensional loading duration in [10] of $\tau = \tau_d$ corresponds to a time T of 1.53 ms. All other material properties correspond to those listed in Table 1 and plotted in Fig. 1.

Consider the situation illustrated in Fig. 4 for time t such that $0 \le t \le T$. There are two waves travelling through the foam core. The elastic precursor travels through the foam and loads it to the elastic limit, σ_P of Fig. 1. The speed of this wave is c_0 and the change in particle velocity associated with this wave is V_Y, where

$$c_0 = \sqrt{\frac{E}{\rho_0}} \approx 653 \text{ m.s}^{-1} \tag{40}$$

$$V_Y = \frac{\sigma_P}{\sqrt{E\rho}} \approx 24 \text{ m.s}^{-1} \tag{41}$$

Behind this elastic precursor there is a slower travelling compaction front that has a speed relative to the elastically loaded material defined from Eqn. (35). The material in the compacted region is loaded to a stress equal to P. Eqns. (37) and (39) give the strain and particle velocity behind the compaction front. The position of the compaction front at the end of stage 1 can be calculated using

$$X_1 = V_S T = T\left(V_Y + \frac{[v]}{[\varepsilon]}(1-\varepsilon_Y) \right), \tag{42}$$

ACCEPTED MANUSCRIPT

where V_S is the absolute velocity of the shock defined in Eqn (33) and the quantity changes are those associated with the compaction wave. The displacement of the proximal end at the end of phase 1 is

$$u_1 = (V_Y + [v])T \,. \tag{43}$$

The total mass of the compacted portion of the material at the end of stage 1 is

$$m_1 = A_0 \rho_A c_S T = A_0 \rho_0 \frac{[v]}{[\varepsilon]} T \,. \tag{44}$$

4.1.2 Stage 2 for *E-P-P-H* shock model

At τ = 1, the elastic precursor reaches the distal end of the foam column and is reflected back as a compaction wave. The jumps in stress, strain and particle velocity and shock wave speed at this distal end are simple to calculate since the elastic precursor has increased the particle velocity to V_Y and the compaction wave brings the material back to rest. Note that this solution is an idealisation based on the *E-P-P-H* model and that experimentally, distal end compaction is often not present. Note also that the stress at the distal end will be greater than σ_P. However, the stress jump at this end is small and corresponds to an increase in stress from 0.8 MPa to 0.84 MPa for this material.

At the same instant that the elastic wave is reflected back as a compaction front at the distal end, the pressure is released at the proximal end. During stage 2, the proximal end can be considered as consisting of an unloading rigid mass of compacted foam that has sufficient velocity to cause further material to compress at this end, i.e. the initial mass at the proximal end is defined in Eqn. (44). The situation in stage 2 is illustrated in Fig. 10. The compaction front at the proximal end is travelling into material in region II that has been loaded to the yield stress and has a particle velocity

ACCEPTED MANUSCRIPT

defined in Eqn. (41). The simplest way to obtain the end displacement and wave positions as a function of time is to consider the material inside the dashed box in Fig. 10. This box moves to the right with a constant speed equal to V_Y so that no material enters or leaves the box over the time increment δt. The compaction front travels to the right with a speed greater than V_Y so that the mass of the compacted portion of the foam increases by an amount δm over the time increment δt. The material in region II has been raised to the yield stress so that the change of momentum of the material inside the box can be related to the impulse delivered at the boundary of the box as

$$\left(m_1 + m + \delta m\right)\left(v + \delta v\right) - \left(m_1 + m\right)v - \delta m.V_y = -A_0\sigma_P\delta t\ . \tag{45}$$

Re-arranging Eqn. (45) and combining this expression with Eqns. (36) and (39) it is possible to define velocity changes as a function of v and Z only, i.e.

$$\frac{\delta v}{\delta t} = \frac{-\left(\sigma_P + \dfrac{\rho_0\left(v - V_Y\right)^2}{\left(\varepsilon_D - \varepsilon_Y + 0.00105\left(v - V_Y\right)\right)}\right)}{\left(\dfrac{m_1}{A_0} + \dfrac{\rho_0}{1-\varepsilon_Y}Z\right)} \tag{46}$$

A solution can then be obtained by solving three first order partial differential equations in terms of the proximal end velocity v (Eqn. (46)), the length Z (Eqn. (36)) and the displacement of the proximal end u ($\delta u/\delta t = v$). The initial conditions for stage 2 come from the final conditions from stage 1. The compaction front at the proximal end will continue to propagate until either full densification occurs or the particle velocity in region III has reduced to the level in region II (see Fig. 10). As the compaction wave propagates, its position can be calculated using

$$X = Z + V_Y\left(t - T\right) + X_1\ , \tag{47}$$

where X_1 is the position at the end of stage 1.

ACCEPTED MANUSCRIPT

4.2 Compaction waves predicted by the *R-P-P-L* and the *E-P-P-H* shock waves and the mass-spring model

As mentioned previously, there are large differences between the "shock-wave" and mass-spring predictions. For "shock-wave" models, stress enhancement never occurs during the propagation of the compaction front through the material. The maximum stress in the foam is equal to the applied pressure during stage 1 and reduces to the plateau stress as the velocity reduces in stage 2. For "shock wave" models the only source of stress enhancement is reflection of the compaction front from the distal end. Other differences between the "shock-wave" and mass-spring predictions are highlighted by inspection of the wave propagation predicted by the two types of analysis. For Example 2, an *R-P-P-L* shock wave solution is plotted in Fig. 11(a). This solution was obtained by solving for u in Eqn. (7) and using Eqn. (2) to find the position of the compaction front. The material in region *I* of Fig. 11(a) is not compressed while the material in region *II* is compacted to the densification strain. Full densification does not occur for this case since nearly 10% of the column is still in region *I* when the compacted portion of the material is brought to rest after about 6.9 ms. The *R-P-P-L* shock wave solution therefore predicts that the pressure applied to the proximal end is attenuated by the foam column and the stress at the distal end never rises above the foam's plateau stress. The solutions in Fig. 11 were obtained via a coordinate system in which the proximal end at $t = 0$ is the origin and the distal end of the column was 1 m from the impact. This axis has been reversed for the plots in Fig. 11 so that the results can be compared more easily with those in Fig. 12 [10]. In Fig. 12, the dimensionless displacement of each mass in a mass-spring model with ten elements is plotted against dimensionless time. The mass-spring prediction is that

ACCEPTED MANUSCRIPT

the compaction wave reaches the distal end and the distal stress is enhanced by the foam column.

The wave locations for the *E-P-P-H* solution are shown in Fig. 11(b). The material in region *I* is unstressed and has no particle velocity. The material in region *II* has been stressed to the elastic limit and has a particle velocity V_Y. The material in regions *III* and *IV* have been compressed beyond ε_D. The solution has been determined until the particle velocity in region *III* has been reduced to that in region *II* at a time of approximately 6.1 ms. At this time 8% of the foam column has no permanent deformation. An elastic unloading wave is now released from the location of the proximal end compaction front and although further compression will occur (see [6]), equating the kinetic energy remaining in the system to the "quasi-static" energy absorption capacity remaining in the foam shows that full densification will not take place.

The *E-P-P-H* solution differs from the *R-P-P-L* solution in two obvious ways. First, reflection of the elastic precursor results in compression from the distal end. Second, the compressive strains in region *III* of Fig. 10(b) are clearly much greater than those in region *II* in Fig. 10 (b). However, there are clear similarities in the solutions and both produce the same conclusion for Example 2, i.e. full densification does not occur so that the pressure pulse applied to the proximal end is attenuated by the foam column.

Clearly the results differ greatly with those for the mass-spring model. The compaction wave in Fig. 12 shows very little reduction in velocity. However, the point masses within the compacted region apparently change speed a number of times

ACCEPTED MANUSCRIPT

after the compaction wave has passed beyond the mass. This oscillation is not seen in the "shock-wave" models and is the cause of the stress histories shown in [10] where there is more than one peak stress within the compaction wave. Early studies on mass-spring models [25] show a succession of saddles and peaks that correspond to the post-yield deformation characteristics of the cells, even for low velocity impacts. The number of peaks in the load-history is directly related to the number of cells that are crushed. However, the oscillations in stress and displacement reported in [10] are unusual. The strength of these mass-spring models is their ability to incorporate a wide variety of material properties and a variation in strength from one cell to the next. However, their ability to simulate stress wave fronts (shock or non-shock) in a material depends on the discretisation levels used. Large amplitude vibrations may result from insufficient discretisation and these vibrations can be misinterpreted as stress enhancements.

Another obvious difference is that Fig. 12 shows masses "pulling away" from the back of the proximal end. This is not seen in the results reported in [11], nor in the "shock-wave" solutions, where unloading behaviour is not considered and compacted portions of material will remain at their maximum strain throughout the solution, even when the stress reduces (rigid unloading). This omission in the "shock-wave" solution may lead to errors for the pressure pulse loading situation, however this should not be significant for other loading situations where impact masses, facesheets *etc*. prevent separation of the material during unloading.

The inclusion of elasticity is unlikely to lead to large differences in the "shock-wave" prediction of Fig. 6, but will lead to a decrease in the critical time period calculated

ACCEPTED MANUSCRIPT

for a *R-P-P-L* material from Eqn. (30). On the other hand, the inclusion of a more accurate model beyond the onset of densification will lead to increased predictions for this critical period. Overall, the large differences between the predictions for the enhancement/attenuation boundary shown in Fig. 6 are not likely to be the result of the simplified *R-P-P-L* material model used in the shock theory. Rather, the difference is due to the fundamental difference (explained below) in the way that the compaction wave is modelled.

4.3. Discussion of mass-spring and alternative models for shock propagation

Mass-spring models have certain similarities to those FE models that incorporate a cellular structure for the material [4, 20-21]. Both types of analysis make use of lumped masses as well as elements that represent the strength of the solid phase of the material. Furthermore, some FE predictions (for example those based on two-dimensional honeycombs) have been shown to agree well with "shock wave" theory [4, 24].

However the fundamental difference between the mass-spring and FE models that incorporate a cellular structure for the material is that the loading path is defined in the mass-spring models that have been described in the literature to date, wherein the quasi-static stress-strain curve is always assumed to be followed within each individual cell. This is similar to the Scheme 2 prediction considered for example 1 and herein lies the error. As noted earlier, the speed of the compaction wave derived from the mass-spring model in [11] is compared to the speed predicted by "shock theory". The argument in [11] is that the close agreement between the compaction wave speeds predicted by the two methods verifies the accuracy of the mass-spring system. However, only low pressures are considered in [11] and differences in

ACCEPTED MANUSCRIPT

predictions will increase with increasing "jumps" in particle velocity. Furthermore, the close agreement in terms of compaction wave speeds is simply because this wave-speed is highly dependent on the impact velocity and the stress-strain relationship within the densification region. The "extra" energy absorbed due to dynamic compression in [11] is simply the consequence of the cell being compressed further along the quasi-static loading path. Alternatively, the "extra" energy absorbed in a "shock" results from the material following a *different* loading path to the quasi-static response. As such, the compaction wave in the mass-spring models is of a different nature to that in "shock-wave" theory. The one-dimensional mass-spring models reported in [10, 11] are not capable of modelling the discontinuities that would exist in a shock in a cellular material. Even if viscous damping effects *etc.* are included in a mass-spring model, the result is that a loading-path-dependent solution is defined. In contrast, when FE models that incorporate a cellular structure for the material are loaded dynamically, inertial effects can lead to deformation modes that differ from those for quasi-static compression.

This is a fundamental problem and applies to all situations where shock behaviour is required by the physics of the problem. The examples above have been kept simple in order to highlight the differences between the different analytical approaches. For example, the boundary conditions affecting the interaction between the foam and the agent producing the blast are unrealistic compared to those for a real blast situation. Further details on the effect of fluid-structure interaction on the pressure pulses applied to structures during blast loading can be found in [26] for blasts in water and [27] for blasts in air. Also herein, the cellular materials have been treated as a continuum and deformations are assumed to occur at wavefronts. Clearly this is not

ACCEPTED MANUSCRIPT

always the case (e.g. see [28]) and sufficient particle velocity must be reached before a "steady" compaction wave is formed [4]. A recent FE study that employs a hexagonal cell structure [24] gives predictions that agree closely with "shock-wave" theory and suggests that the compaction front has a dimension of approximately one cell size. This is in agreement with the experimental evidence available [29].

The material properties that are needed to predict the shock compression of cellular materials are ill-defined. "Equations of state" for solid materials are normally derived from e.g. plate-impact test data. Equivalent data for compaction waves in cellular materials are not available due to the difficulties associated with measuring the "states" either side of a compaction wave. Currently, quasi-static stress-strain curves are used to predict stresses under impact conditions. These quasi-static material properties are usually measured over length scales over which several cells are present in any direction and deformation modes are very different to those during dynamic compaction. This issue will be the subject of future research

5. Conclusions

Two examples of the dynamic compression of a cellular material have been analysed. It has been shown that the 'correct' shock theory solution can be derived purely by applying the conservation equations for mass and momentum and this derivation has been used to explain differences between "shock" solutions available in the literature. An extended shock theory, which accounts for the non-lineartity in the post-locking behaviour of the material, has been derived and compared to the predictions of a mass-spring model for the case of rectangular pressure pulse loads.

ACCEPTED MANUSCRIPT

The mass-spring model in [10] predicts that stress enhancements can occur during the propagation of a compaction wave through a cellular material. The "shock theory" prediction is that the stress in the compacted-region is constant at P during stage 1 and then reduces below this value during stage 2, i.e. the stress in the foam only exceeds the magnitude of the applied pressure once the entire foam column is fully compacted. For pressures of between two and five times the plateau stress in the foam, there is a large difference in the predictions of the "mass-spring" and "shock wave" models. The predictions are expected to diverge as the loading intensity increases.

"Shock theory" has been shown to predict well experimental results for a number of cellular materials (e.g. [6]) and to be in close agreement with FE simulations (e.g. [24]). However "mass-spring" models have not been calibrated against test data for cases where compaction waves are likely to occur. As such, the authors believe that "mass-spring" models should be treated with caution.

ACCEPTED MANUSCRIPT

References

[1] Reid SR and Peng C. Dynamic Uniaxial Crushing of Wood. Int. J. Impact Engng. 1997(5-6); 19, 531-570.

[2] Tan PJ, Harrigan JJ, Reid SR. Inertia effects in uniaxial dynamic compression of a closed cell aluminium alloy foam. Mater Sci Technol 2002;18:480–488.

[3] Tan PJ, Reid SR, Harrigan JJ, Zou Z and Li S. Dynamic compressive strength properties of aluminium foams. Part I – Experimental data and observations, J Mech. Phys Solids 2005; 53:2174-2205.

[4] Tan PJ, Reid SR, Harrigan JJ, Zou Z and Li S. Dynamic compressive strength properties of aluminium foams. Part II – Shock theory and comparison with experimental data, J Mech. Phys Solids 2005; 53: 2206–2230.

[5] Harrigan JJ, Reid SR, Reddy TY. Inertia effects on the crushing strength of wood loaded along the grain. In: Allison IM,editor. Experimental mechanics. Rotterdam: Balkema; 1998. p. 193–198.

[6] Harrigan JJ, Reid SR, Tan PJ and Reddy TY. High rate crushing of wood along the grain, Int J Mech Sci 2005; 47:521-544.

[7] Hanssen AG, Enstock L, Langseth M. Close-range loading of aluminum foam panels. Int J Impact Eng 2002;27:593–618.

[8] Lopatnikov SL, Gama BA, Haque MJ, Krauthauser C, Guden M, Hall IW, Gillespie JW. Dynamics of metal foam deformation during Taylor cylinder – Hopkinson bar impact experiment. Compos Struct 2003;61:61–71.

[9] Lopatnikov SL, Gama BA, Haque MJ, Krauthauser C, Gillespie Jr JW. High-velocity plate impact of metal foams. Int J Impact Eng 2004;30(4):421–445.

[10] Li QM, Meng H. Attenuation or enhancement–a one-dimensional analysis on shock transmission in the solid phase of cellular material. Int J Impact Eng 2002;27:1049–65.

[11] Z. Y. Gao and T. X. Yu, One-dimensional analysis on the dynamic response of cellular chains to pulse loading, Proc. Inst. Mech. Engrs., Part C: J. Mech. Eng. Sci. 2006;220:679-689.

ACCEPTED MANUSCRIPT

[12] Ashby MF, Evans A, Fleck NA, Gibson LJ, Hutchinson JW and Wadley HNG. Metal foams: A design guide. Butterworth Heinemann, London, 2000.

[13] Lu, Guoxing, and Yu, Tongxi. Energy absorption of structures and materials. Woodhead Publishing Ltd., Cambridge, 2003.

[14] Fleck NA and Deshpande VS. The resistance of clamped sandwich beams to shock loading. J. Appl. Mech. 2004;71(3):386-401.

[15] Tan P J, Reid SR and Harrigan JJ. Discussion: "The resistance of clamped sandwich beams to shock loading" (Fleck, N.A., Deshpande, V.S., 2004, ASME J. Appl. Mech., 71, pp. 386 – 401). J. Appl. Mech. 2005;72:978-979.

[16] Fleck NA and Deshpande VS. Closure to "Discussion of 'The Resistance of Clamped Sandwich Beams to Shock Loading' " (2005, ASME J. Appl. Mech., 72, pp. 978–979). J. Appl. Mech. 2005;72:980.

[17] Li QM and Reid SR. About one-dimensional shock propagation in a cellular material. Int J Impact Eng 2006;32:1898–1906.

[18] Qiu X, Deshpande VS, Fleck NA. Dynamic response of a clamped circular sandwich plates to shock loading. J Appl Mech 2004;71:637-645.

[19] Li QM, Mines RAW, Birch RS. The crash behaviour of Rohacell-51WF foam. Int J Solids Struct 2000;37:6321–41.

[20] Ruan D, Lu G, Wang B, Yu TX. In-plane dynamic crushing of honeycombs – finite element study. Int J Impact Engng 2003; 28:161-182.

[21] Zheng Z, Yu J, Li J. Dynamic crushing of 2D cellular structures: A finite element study. Int J Impact Engng 2005; 32:650-664.

[22] Harrigan JJ, Hung YC, Tan PJ, Bourne NJ, Withers PJ, Reid SR, Millett JCF, Milne AM. High rate compaction of aluminium alloy foams, in Shock Compression of Condensed Matter – 2005, Eds. M.D. Furnish, M. Elert, T.P. Russell and C.T. White © 2006 American Institute of Physics, Pages: 1519-1522, ISSN/ISBN: 0-7354-0341-4.

[23] Li QM, Magkiriadis I, Harrigan JJ, Compressive strain at the onset of the densification of cellular solids, J. Cellular Plastics 2006(5); 42: 371-392.

ACCEPTED MANUSCRIPT

[24] Zou Z, Reid SR, Tan PJ, Li S, Harrigan JJ, Dynamic crushing of honeycombs and features of shock fronts, International Journal of Impact Engineering, Int J Impact Engng 2009; 36:365-176.

[25] Shim, V. P. W., Tay, B. Y., and Stronge, W. J. Dynamic crushing of strain-softening cellular structures – a one dimensional analysis. J. Eng. Mater. Technol. 1990, 112, 398–405.

[26] Deshpande VS and Fleck NA. One-dimensional response of sandwich plates to underwater shock loading. J. Mech. Phys. Solids 2005;53:2347–2383.

[27] Kambouchev N, Noels L and Radovitzky R. Nonlinear compressibility effects in fluid-structure interaction and their implications on the air-blast loading of structures, J Appl. Phys. 2006;100:063519.

[28] S. McKown, Y. Shen, W.K. Brookes, C.J. Sutcliffe, W.J. Cantwell, G.S. Langdon, G.N. Nurick and M.D. Theobald, The quasi-static and blast loading response of lattice structures, Int J Impact Eng 2008; 35: 795–810

[29] Radford DD, Deshpande VS, Fleck NA. The use of metal foam projectiles to simulate shock loading on a structure. Int J Impact Engng 2005; 31:1152-1171

ACCEPTED MANUSCRIPT

List of tables:

List of figures:

ACCEPTED MANUSCRIPT

Table 1. Mechanical properties of Rohacell-51 WF foam.

ρ_0 (kg.m^{-3})	E (MPa)	σ_P (MPa)	ε_y (%)	ε_D (%)
51.6	**22.0**	**0.8**	**3.64**	**68.9**

ACCEPTED MANUSCRIPT

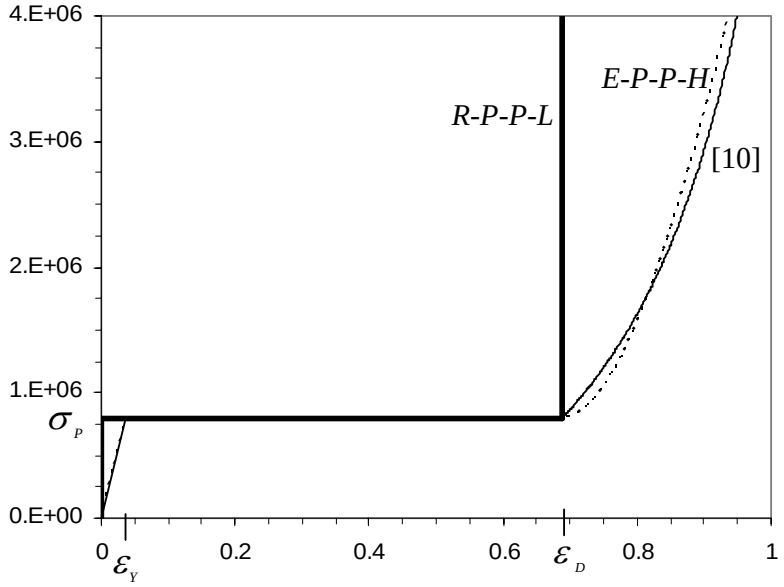

Fig. 1. Stress-nominal strain from [10] together with *R-P-P-L* and *E-P-P-H* material models.

ACCEPTED MANUSCRIPT

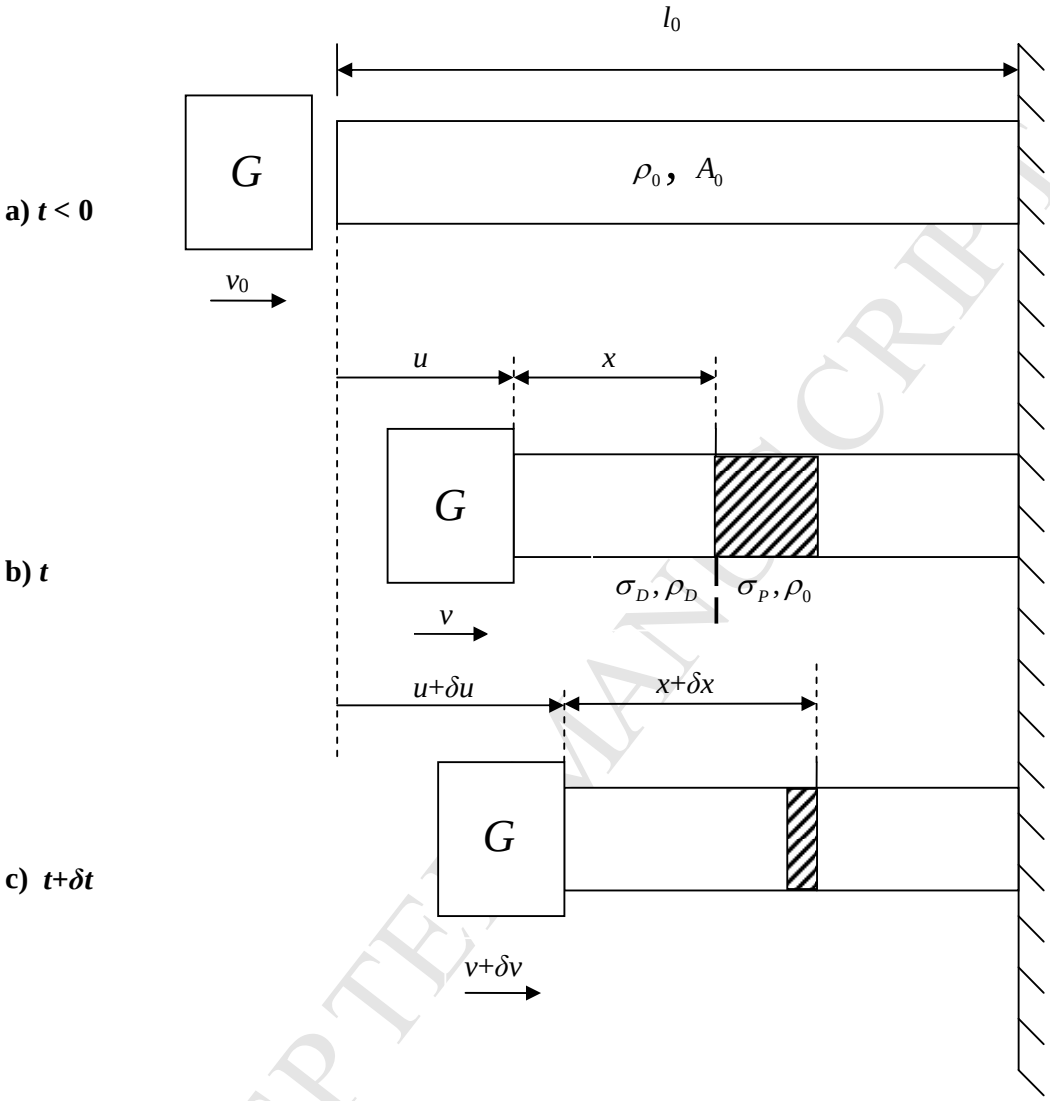

Fig. 2. Example 1: A mass *G* impacting a foam column.

ACCEPTED MANUSCRIPT

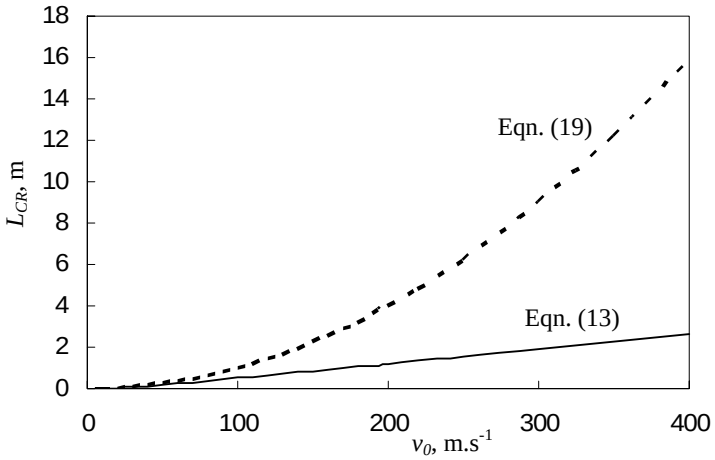

Fig. 3. Comparison between critical lengths for the two solution schemes for G = 40 kg, A_0 = 1 m^2, ε_D = 0.67, σ_0 = 0.3 MPa and ρ_0 =155 Kg.m^{-3}.

ACCEPTED MANUSCRIPT

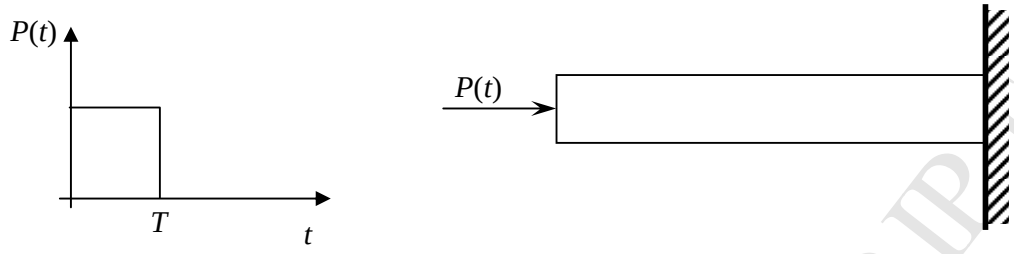

Fig. 4. Example 2: Rectangular pressure pulse applied to foam column.

ACCEPTED MANUSCRIPT

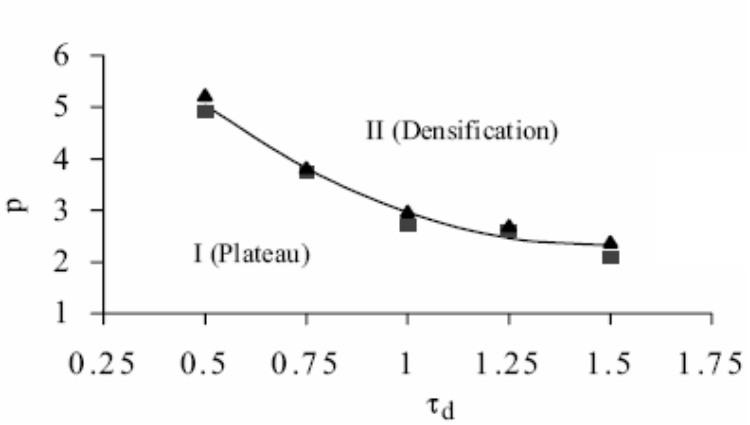

Fig. 5. Non-dimensional enhancement/attenuation boundary according to Li and Meng [10]. Squares denote densification. Triangles denote distal stresses greater than the applied pressure.

ACCEPTED MANUSCRIPT

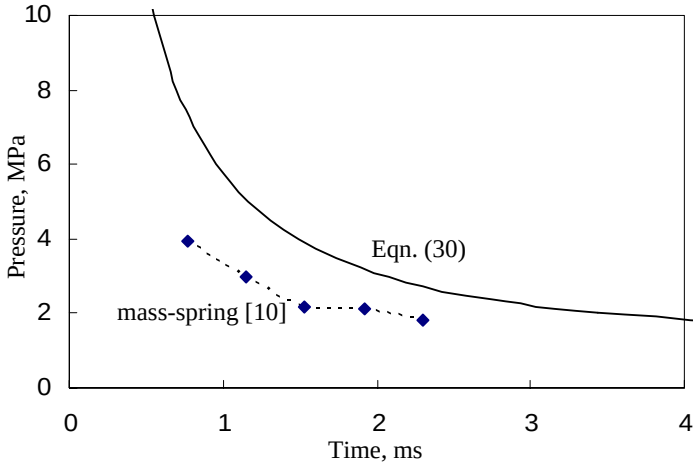

Fig. 6. Enhancement/attenuation boundaries for a 1 m long Rohacell-51 WF foam column according to "shock theory" and a mass-spring model [10].

ACCEPTED MANUSCRIPT

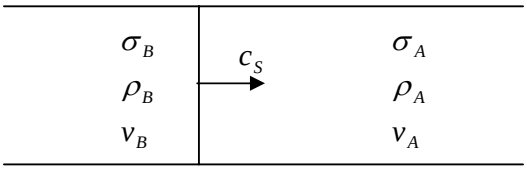

Fig. 7. States immediately ahead of and behind a one-dimensional shock.

ACCEPTED MANUSCRIPT

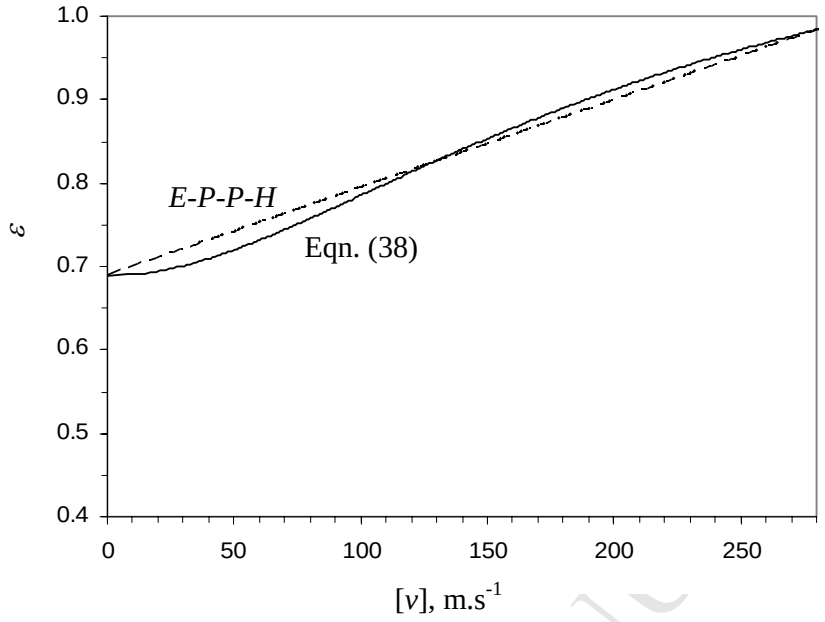

Fig. 8. Strain-particle velocity relationship corresponding to Eqn. (38) and *E-P-P-H* material models.

ACCEPTED MANUSCRIPT

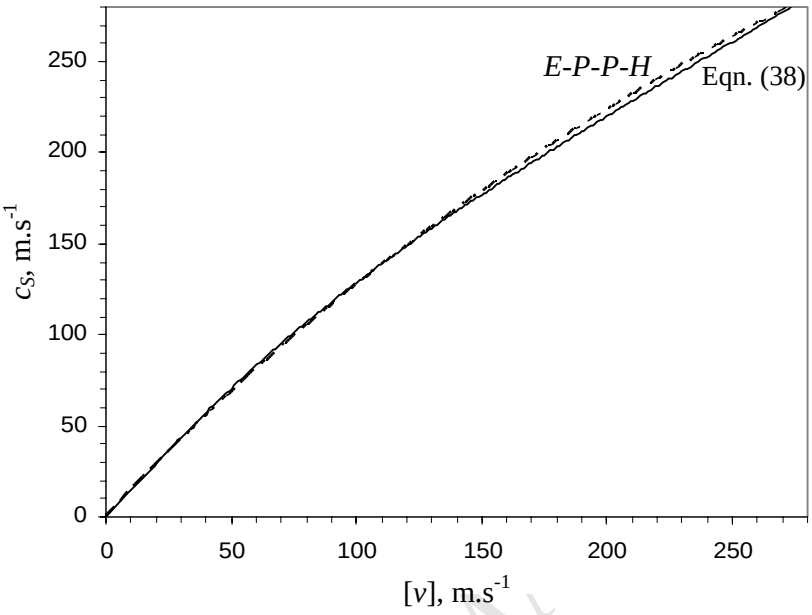

Fig. 9. Shock speed-particle velocity relationship corresponding to Eqn. (38) and *E-P-P-H* material models.

ACCEPTED MANUSCRIPT

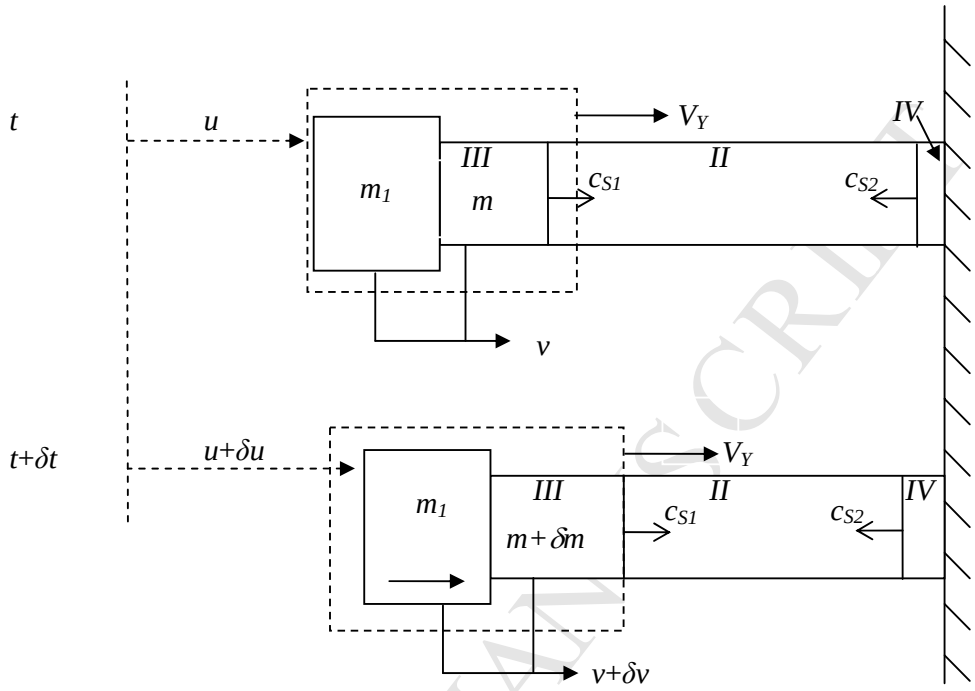

Fig. 10. Example 2: Stage 2 for *E-P-P-H* material model.

ACCEPTED MANUSCRIPT

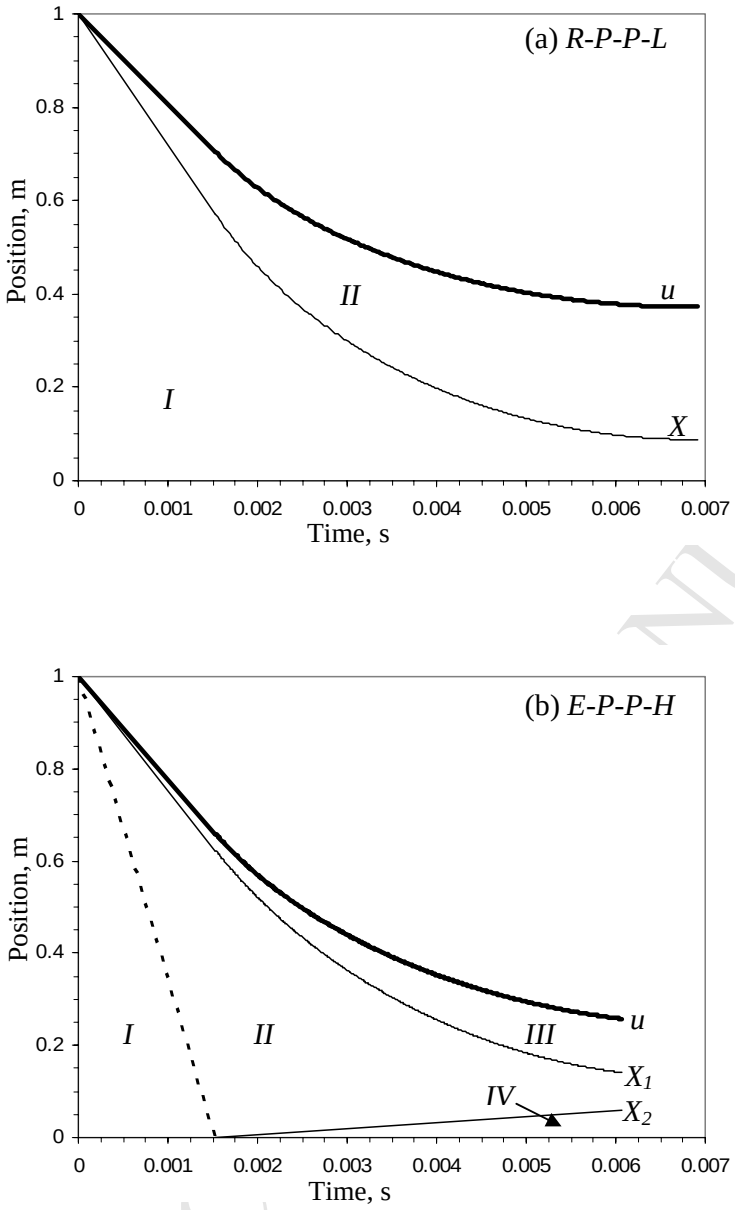

Fig. 11. Propagation of elastic and compaction waves according to "shock-wave" theory for (a) *R-P-P-L* and (b) *E-P-P-H* material models.

ACCEPTED MANUSCRIPT

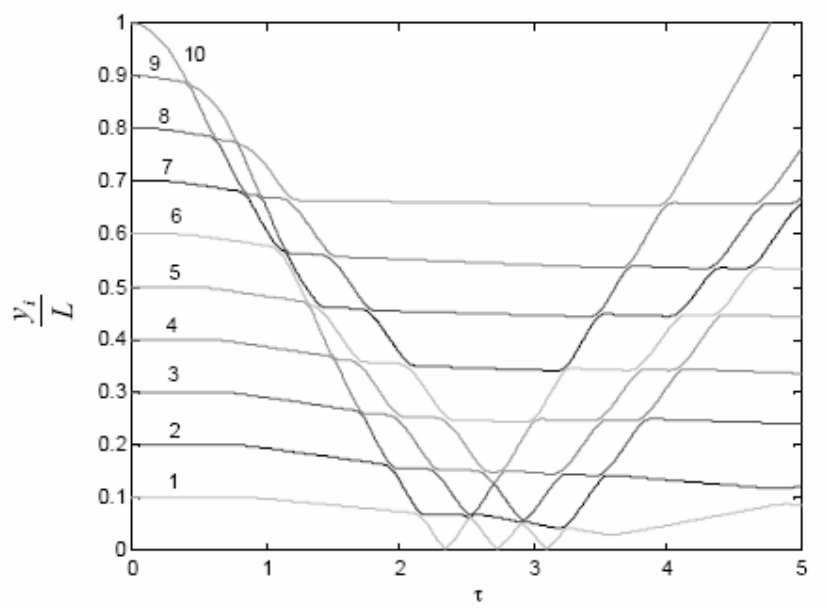

Fig. 12. Propagation of elastic and compaction waves according to mass-spring model [10]. Each line shows the dimensionless position of a point mass as a function of dimensionless time.

ACCEPTED MANUSCRIPT